ACS NANO

www.acsnano.org

ARTICLE

Scalable Indium Phosphide Thin-Film Nanophotonics Platform for Photovoltaic and Photoelectrochemical Devices

Qingfeng Lin,[†] Debarghya Sarkar,[†] Yuanjing Lin,[‡] Matthew Yeung,[†] Louis Blankemeier,[†] Jubin Hazra,[†] Wei Wang,[†] Shanyuan Niu,[§] Jayakanth Ravichandran,[§] Zhiyong Fan,[‡] and Rehan Kapadia*[,†]

[†]Ming Hsieh Department of Electrical Engineering, University of Southern California, Los Angeles, California 90089, United States

[‡]Department of Electronic and Computer Engineering, The Hong Kong University of Science and Technology, Clear Water Bay, Kowloon, Hong Kong SAR, China

[§]Mork Family Department of Chemical Engineering and Materials Science, University of Southern California, Los Angeles, California 90089, United States

Supporting Information

ABSTRACT: **Recent developments in nanophotonics have provided a clear roadmap for improving the efficiency of photonic devices through control over absorption and emission of devices. These advances could prove transformative for a wide variety of devices, such as photovoltaics, photoelectrochemical devices, photodetectors, and light-emitting diodes. However, it is often challenging to physically create the nanophotonic designs required to engineer the optical properties of devices. Here, we present a platform based on crystalline indium phosphide that enables thin-film nanophotonic structures with physical morphologies that are impossible to achieve through conventional state-of-the-art material growth techniques. Here, nanostructured InP thin films have been demonstrated on non-epitaxial alumina inverted nanocone (i-cone) substrates *via* a low-cost and scalable thin-film vapor−liquid−solid growth technique. In this process, indium films are first evaporated onto the i-cone structures in the desired morphology, followed by a high-temperature step that causes a phase transformation of the indium into indium phosphide, preserving the original morphology of the deposited indium. Through this approach, a wide variety of nanostructured film morphologies are accessible using only control over evaporation process variables. Critically, the as-grown nanotextured InP thin films demonstrate excellent optoelectronic properties, suggesting this platform is promising for future high-performance nanophotonic devices.**

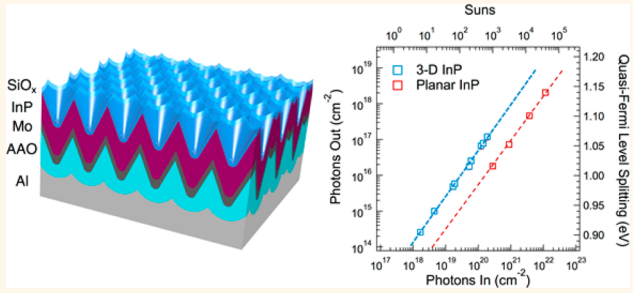

KEYWORDS: *indium phosphide, thin film, nanophotonics, low-cost and scalable, photonic devices*

Engineering the absorption and emission characteristics of photovoltaic and photoelectrochemical devices is critical for maximizing solar harvesting device performance.[1−11] Presently, optical engineering approaches for thin-film devices rely on amorphous thin films deposited on nanopatterned substrates.[12−19] Whereas this approach has demonstrated excellent performance enhancements of solar cells and is low-cost, the use of amorphous or nanocrystalline semiconductors severely limits the ultimate performance of these devices when compared to those made from large-grain polycrystalline and single-crystalline materials.[20−24] Combining the performance enhancements enabled by nanophotonic engineering with low-cost crystalline semiconductors would be an enabling tool in the development of high-performance low-cost solar energy harvesting devices. However, the kinetics of traditional vapor−solid material growth approaches severely limit the control over the film geometry on non-epitaxial substrates,[25−30] preventing device designers from engineering the films into the desired structures. Here, we introduce a general platform that works around the fundamental kinetic constraint of vapor−solid growth by using a 3-D liquid template to grow high-quality crystalline indium phosphide in user-tunable geometries on non-epitaxial substrates. InP is chosen here as it plays a critical role in both optoelectronic and electronic systems and possesses electronic properties that make it ideal for solar energy harvesting.[31−35] Furthermore, anodized aluminum oxide is chosen here as a substrate due to

Received: March 28, 2017
Accepted: May 2, 2017
Published: May 2, 2017

DOI: 10.1021/acsnano.7b02124
ACS Nano 2017, 11, 5113−5119

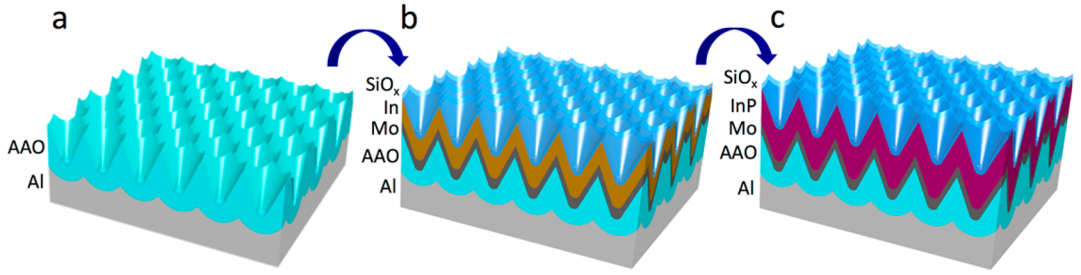

Figure 1. Schematic synthesis process of nanostructured InP thin films. (a) AAO i-cone substrate. (b) AAO i-cone substrate with Mo, indium, SiO_x films. (c) The i-cone InP thin films grown on AAO i-cone substrate.

its scalability and ability to generate nanostructures through low-cost electrochemical processing.[36−41]

The approach used is analogous to the recently developed thin-film vapor−liquid−solid (TF-VLS) growth technique, which has been demonstrated to produce high-quality, large-grain-size (>100 μm) III−V films on non-epitaxial substrates.[25,42,43] In detail, nanostructured InP films with a variety of morphologies have been demonstrated on alumina inverted nanocone (i-cone) substrates. The as-grown nanostructured InP thin films also showed promising optoelectronic properties. Critically, the TF-VLS growth is scalable as it uses processes identical to those used for large-area CIGS cells, and large-scale AAO processing is widely used for many applications. Here, we are merging two approaches that have both independently been demonstrated to be scalable. Thus, the approach here demonstrates a low-cost III−V thin-film nanophotonics platform for electronic, photonic, and energy applications.

RESULTS AND DISCUSSION

The synthesis process for the InP nanostructured thin films is schematically illustrated in Figure 1. Briefly, the patterned alumina i-cone arrays (Figure 1a) were fabricated on the imprinted Al foil *via* a low-cost and scalable multistep anodization and wet etching process in an acidic solution with a proper direct current voltage.[17,22,40] The detailed fabrication process of the anodic aluminum oxide (AAO) i-cone array is described in the Methods section. Thereafter, 100 nm thick molybdenum (Mo) was sputtered onto the AAO i-cone substrate followed by thermal evaporation of indium (In) films of varying thicknesses, which was subsequently encapsulated by 30 nm thick SiO_x film *via* electron-beam (e-beam) evaporation, as shown in Figure 1b. Note that the Mo layer serves multiple purposes here. First, it has been previously established that indium thin films between Mo substrates and SiO_x capping layers do not dewet when heated above the indium melting point (167 °C), enabling the liquid indium to maintain the as-deposited shape.[42] Second, the Mo film can work as a nucleation substrate for the growth of InP. Third, the Mo solubility in liquid indium at the growth temperatures is low minimizing contamination. Growth of the nanostructured InP thin films was performed in a chemical vapor deposition (CVD) furnace in the presence of 0.2% phosphine (PH_3) in hydrogen (H_2) at 600 °C under 100 Torr pressure.

At the growth temperature, the indium is in the liquid phase, but the Mo and SiO_x layers enable it to remain in the as-deposited shape, which is the key feature that enables this growth. Therefore, control over the final InP geometry is carried out by tuning the geometry of the deposited indium. The phosphorus enters the liquid indium through pinholes in the evaporated SiO_x layer, causing supersaturation of the liquid indium, leading to the precipitation of solid InP crystals. This process resembles the self-catalyzed vapor−liquid−solid (VLS) growth of nanowires closely but has been previously shown to result in continuous polycrystalline thin films (Figure 1c) instead of nanowires.[29,42] The as-grown InP thin films *via* this technique have been previously shown to have ultralarge grain sizes on the order of hundreds of micrometers.[42,43] Furthermore, since the geometry of the InP thin films is controlled by the geometry of the initial indium, this approach offers the ability to tune the geometry of the grown nanostructured InP thin films.

As the resulting morphology of the InP thin films is dictated by the deposited indium, it is critical to investigate the range of film morphologies possible to achieve. In this work, the indium thin films were thermally evaporated on the Mo coated i-cone substrates. The varied morphologies were then achieved by tuning the (i) substrate temperature during evaporation and (ii) the evaporation rate. Specifically, when conformal films were desired, the substrate was held at low temperature (~120 K) because indium tended to dewet if it was evaporated on the substrate at room temperature (Figure S1a,b). Next, a SiO_x layer was evaporated on the indium films by e-beam evaporation as a capping layer to enable templating of the liquid indium at the growth temperature. Figure 2 shows 45°-tilted-view (Figure 2a,c,e) and cross-sectional (Figure 2b,d,f) scanning electron microscope (SEM) images of indium thin films with different morphologies on various i-cone substrates. Note that all the AAO i-cone arrays presented in this work have a periodicity of 1 μm. Conformal i-cone thin films (Figure 2a,b) with a thickness of 200 nm were achieved on 250 nm deep i-cone substrates *via* an evaporation rate of 5 Å/s. It is worth noting that a high evaporation rate would lead to indium nanostructures with sharp edges (Figure S1c,d), as numerous indium particles nucleated vertically in a short time. Split resonant structures (Figure 2c,d) were obtained on 500 nm deep i-cone substrates with the same evaporation condition for conformal films, due to the steep surface of the 500 nm deep AAO i-cone arrays. Moreover, independent top and bottom surfaces (Figure 2e,f) were demonstrated when a 500 nm thick indium layer and 100 nm thick SiO_x layer were evaporated on 1 μm deep i-cone substrates. These diverse indium morphologies were created with only one basic shape—the i-cone. However, with the recent advances in nanopatterning and nanofabrication, it is likely that future work using this approach can lead to a significant variety of indium films morphologies suitable for a wide range of applications.

Using the nanotextured indium thin films, nanotextured InP thin films have been demonstrated in Figure 3. Uniform ultrathin InP nanostructured films have been grown on the i-cone substrates conformally, as shown in Figure 3a−d. This

DOI: 10.1021/acsnano.7b02124
ACS Nano 2017, 11, 5113−5119

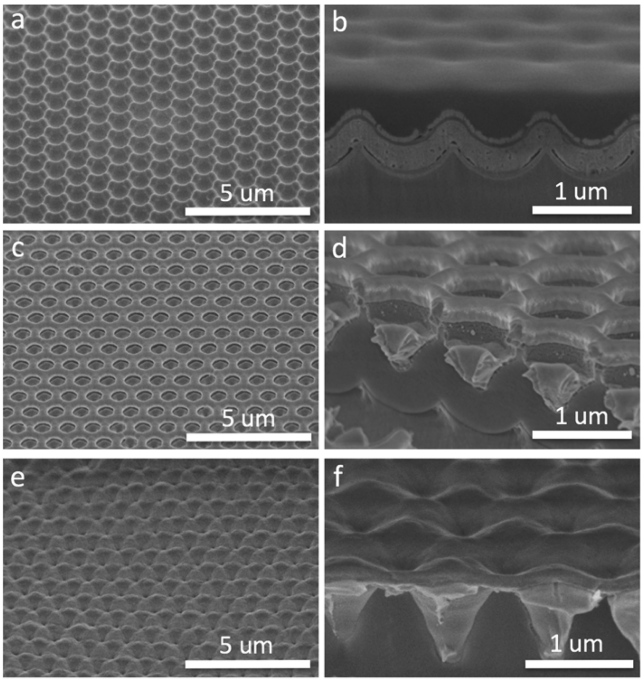

Figure 2. SEM images of indium thin films with different morphologies on various i-cone substrates: (a) 45°-tilted-view and (b) cross-sectional SEM images of conformal i-cone thin films on 250 nm deep i-cone substrates; (c) 45°-tilted-view and (d) cross-sectional SEM images of split resonant structures on 500 nm deep i-cone substrates; (e) 45°-tilted-view and (f) cross-sectional SEM images of independent top and bottom surfaces on 1 μm deep i-cone substrates.

clearly demonstrates that the indium retains the shape of the template even when in liquid form, enabling engineering of the final InP geometry simply by tuning the as-deposited geometry of the indium. Figure 3b–d shows cross-sectional SEM images of nanostructured InP thin films with varying thicknesses (75, 150, and 500 nm, respectively) on the i-cone substrates. Critically, we see that the grown films indeed follow shape of the template, with thicknesses tunable in the <1 μm range. While thicker films are possible,[20,42] they were not explored here. These conformal structures have been previously shown to be significant in light trapping for ultrathin photovoltaics but always used amorphous or nanocrystalline semiconductors.[14−18,44] Thus, this work demonstrates a potentially high-performance semiconductor directly grown in this morphology, which will contribute to the development of low-cost high-performance devices.

Additionally, we demonstrate that other geometry structures can also be grown using this approach. Figure 3e,f demonstrates adjacent cone-shaped structures, again clearly demonstrating that the resulting structures follow the geometry of the as-deposited indium. Interestingly, this approach also enables InP hybrid nanostructures consisting of nanostructured thin films and vapor–solid nanocrystals, as illustrated in Figure 3g,h. To achieve this, the evaporation conditions of the SiO_x were adjusted so that the shadowing effect caused holes in the layer. It is hypothesized that the indium vapor from the sample itself enables this vapor–solid growth mode, even though no indium precursor was introduced into the chamber. These crystals nucleate from the underlying vapor–liquid–solid InP through the holes in the SiO_x capping layer and thus are expected to be of the same crystal orientation as the substrate. Furthermore, as

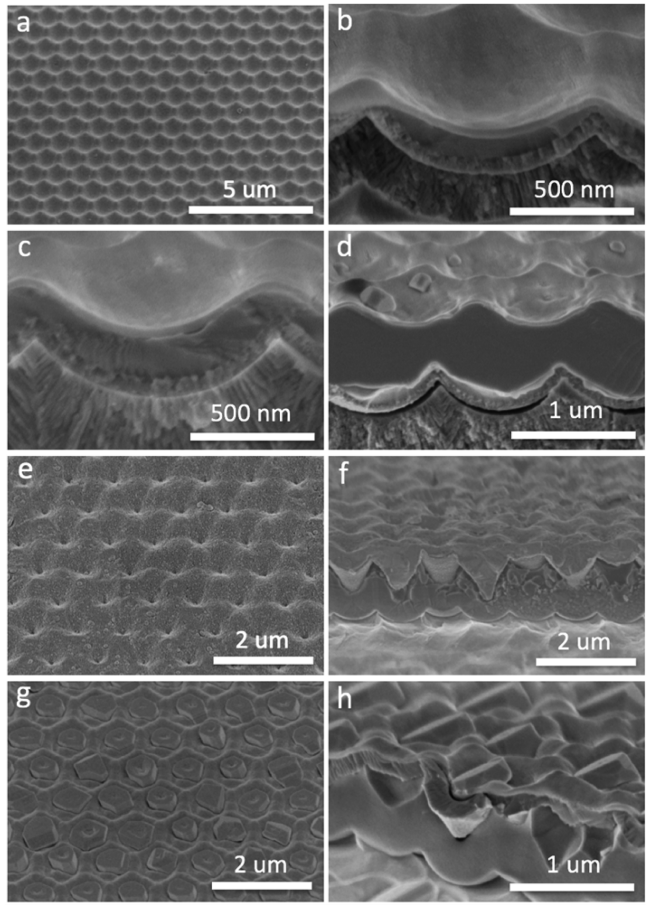

Figure 3. SEM images of nanostructured InP thin films: (a) 45°-tilted-view and (b–d) cross-sectional SEM images of uniform ultrathin InP nanostructured films with varying thicknesses; (e) 45°-tilted-view and (f) cross-sectional SEM images of touching cone-shaped InP nanostructures; (g) 45°-tilted-view and (h) cross-sectional SEM images of InP hybrid nanostructures.

visible from Figure 3h, all the vapor–solid InP crystals grown from the below InP thin films appear to all be pointed in the same direction, suggesting that the slow growth planes of the crystals are aligned and they have a similar crystal orientation. This would be expected given the prior results on the nucleation density and grain size of TF-VLS films grown on Mo under similar conditions.

In order to characterize the material quality of the grown nanostructured InP thin films, X-ray diffraction (XRD) and steady-state photoluminescence (SSPL) spectra were carried out on the nanostructured InP thin films. Note that we performed the characterizations on the 500 nm thick i-cone InP films as shown in Figure 3d. The XRD spectrum (Figure 4a) demonstrates several structural properties of the grown InP thin films. First, the as-grown InP is zinc blende structure. Second, the lack of indium peaks indicates that the indium film has fully transformed into InP. Third, the InP thin films are slightly textured as evident by the relatively stronger 111 peak compared to other peaks, when compared to the standard reference patterns.[45] As the diffraction measurements were performed on InP samples supported on AAO membranes, we see an amorphous background with a broad peak around 25°. We confirmed that this peak was present in AAO membranes before the growth, too. These results provide the structural evidence for presence of zinc blende InP. To determine the

DOI: 10.1021/acsnano.7b02124
ACS Nano 2017, 11, 5113–5119

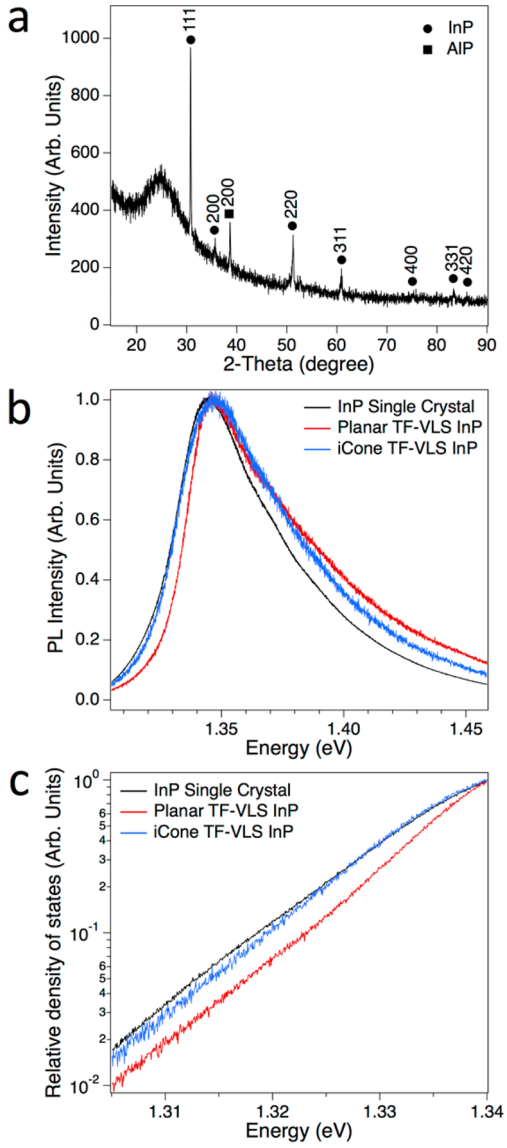

Figure 4. Material quality characterization of nanostructured InP thin films. (a) XRD spectrum of 500 nm thick i-cone InP films. (b) SSPL curves of i-cone TF-VLS InP films, planar TF-VLS InP films, and a single-crystalline n-type InP wafer. (c) Relative density of states of i-cone TF-VLS InP films, planar TF-VLS InP films, and a single-crystalline n-type InP wafer.

optoelectronic properties of the grown films, SSPL was performed to determine the energy position of the peak photoluminescence intensity. A representative SSPL curve of the nanostructured InP is shown in Figure 4b, together with that of planar TF-VLS InP films and a single-crystalline n-type InP wafer as the references. The measurements were carried out at ambient temperature with a 532 nm laser as the excitation source. The nanostructured InP thin film exhibits an SSPL peak position of 1.347 eV and fwhm of 0.056 eV. These results are similar to the single-crystalline reference, which exhibits a peak position of 1.345 eV and a fwhm of 0.049 eV. From the SSPL spectra, we extracted the relative density of states at the band edge, as shown in Figure 4c. The semilog inverse slope of the density of states is related to the Urbach tail parameter (see Methods section), which is an important figure of merit regarding the band edge sharpness arising from crystal defects, thermal vibrations, and charged impurities.[46,47] The Urbach tail parameter of the nanostructured InP is 21.9 mV, which is close to the values of the InP single crystal wafers (17.5 mV) and the planar TF-VLS InP films (21.3 mV). All these results demonstrate the high quality of the nanostructured InP explored here.

As mentioned above, the nanostructured InP is an excellent candidate for high efficiency thin-film solar cells, of which an essential parameter is the open-circuit voltage (V_{oc}).[8,9] The V_{oc} of a semiconductor solar cell under illumination is limited by the difference of the chemical potential between the electron and hole population, defined as the quasi-Fermi level splitting (ΔE_F). Therefore, extraction of ΔE_F allows a quantitative prediction of the upper limit of PV performance of a semiconductor material. ΔE_F can be calculated as[9,48]

$$\Delta E_F = kT \ln(R_{abs} / (\int_0^{2\pi} \int_0^{\pi/2} \int_{-\infty}^{\infty} a(E,\theta) b(E) \cos(\theta) dE d\theta d\phi)) + kT \ln(\eta_{ext}) \quad (1)$$

which is determined by the optical properties of the semiconductor and the measured external luminescence efficiency, η_{ext} = (number of emitted photons)/(number of absorbed photons). The dependence can be qualitatively explained where the only loss mechanism for PV devices to reach the Shockley–Queisser (SQ) limits should be radiative recombination.[49] Hence one photon must be emitted for each photon absorbed (η_{ext} = 100%) at the SQ limits under open-circuit conditions.[8,9] The external luminescence efficiency and quasi-Fermi level splitting were extracted from the obtained output photoluminescence (PL) intensity under varied incident photon illumination. Details of the measurements and analyses can be found in the Methods section. Figure 5 plots power-dependent PL emission intensities of comparable TF-VLS planar and nanostructured InP thin films, with the number of suns corresponding to the incident photon flux labeled on the top horizontal axis. We find that the grown film here not only is of comparable quality with the previously demonstrated InP but also shows an increase of emitted photons at particular incident illumination intensity compared to TF-VLS planar InP

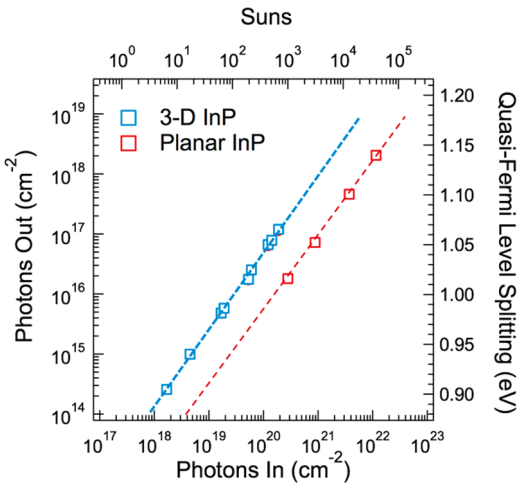

Figure 5. Power-dependent PL emission intensities and quasi-Fermi level splitting of comparable TF-VLS planar and nanostructured InP thin films.

DOI: 10.1021/acsnano.7b02124
ACS Nano 2017, 11, 5113–5119

thin films. The quasi-Fermi level splitting extracted from the integrated PL intensity is shown on the right axis of Figure 5, which shows that the i-cone InP thin films exhibit $\Delta E_F \sim 60$ meV greater than planar InP thin films for the measured excitation intensity range. As high-quality photovoltaic devices have already been made from planar TF-VLS InP,[20,24] this suggests that the platform used here could be used to further improve the quality of those cells.

CONCLUSION

The features of the thin-film vapor−liquid−solid (TF-VLS) process enable the growth of nanostructured InP thin films on nanotextured substrates. It is important to note that the TF-VLS growth technique has significant advantages on fabrication costs over traditional epitaxial growth processes, such as metal organic chemical vapor deposition. Nanostructured InP thin films with a variety of morphologies have been grown directly on scalable, low-cost, non-epitaxial alumina i-cone substrates *via* this technique. Additionally, we have demonstrated that this approach is highly controllable and that design of InP nanostructures is possible, which is of interest for engineering optoelectronic devices. The XRD and SSPL characterization demonstrated the structural and optoelectronic properties of the films. Moreover, the nanostructured InP thin film demonstrated even greater external luminescence efficiency and quasi-Fermi level splitting compared to that of the planar counterpart. These results suggest the platform for nanostructured InP thin films developed here is an ideal candidate for future low-cost high-performance energy harvesting and optoelectronic devices.

METHODS

Fabrication of AAO Inverted Nanocone Arrays. An electrochemically polished Al foil was mechanically imprinted using a silicon stamp with hexagonally ordered nanopillars with 200 nm height and 1 μm pitch to produce nanoindentation arrays on the Al surface. The imprinted Al substrate was first anodized in "230 mL, 1:1, 4 wt % citric acid/ethylene glycol + 15 mL of 0.1 wt % phosphoric acid" with 400 V direct current voltage at 10 °C to form an ordered alumina hole layer, which was then completely removed in a mixture of 6 wt % phosphoric acid and 1.8 wt % chromic acid at 100 °C, resulting in a 250 nm deep Al i-cone substrate. Thereafter, 250 nm, 500 nm, and 1 μm deep alumina i-cone substrates were obtained by more anodization steps, in conjunction with wet etching using 5 wt % phosphoric acid at 53 °C between two anodization steps to widen the alumina i-cone pore size, with their fabrication processes (starting from second anodization) shown in Supporting Information Table S1.

Growth of InP Nanophotonic Films. The prepared AAO/Mo/In/SiO_x samples were placed in a one-zone CVD furnace with a phosphorus source of 0.2% PH_3 (99.9995%) in H_2 (99.9999%) to grow InP nanophotonic films. Specifically, the AAO/Mo/In/SiO_x samples were first heated in a hydrogen environment in the furnace, followed by exposure to the phosphorus source when the furnace stabilized at the growth temperature of 600 °C. Then, the InP nanophotonic films were grown from indium films after being exposed to the phosphorus source for 30 min at the growth temperature under 100 Torr pressure. Finally, the as-obtained AAO/Mo/InP/SiO_x samples were taken out from the furnace after cooling (~10 min) to room temperature.

Structural Characterization. The powder XRD characterization was carried out using a Bruker D8 Advance X-ray diffractometer with Co Kα radiation in Bragg−Brentano symmetric geometry with power setting of 35 kV and 40 mA. The sample stage was rotated at 15 rpm. The scan was taken from 15 to 90° with a 0.02° step and 1 s integration time for each data point.

Urbach Tail Fitting. The van Roosbroeck−Schockley equation relates the band-edge absorption coefficient to the photoluminescence spectrum, and thus the density of states can be represented as[50]

$$D(\nu) \propto \frac{I(\nu)(\exp(h\nu/kT) - 1)}{\nu^2} \propto \exp\left(\frac{h\nu - E_g}{E_0}\right) \quad (2)$$

where $I(\nu)$ is the photoluminescence intensity as a function of frequency ν, h is Planck's constant, and kT is the thermal energy (25.6 mV at room temperature). E_0 is the Urbach tail parameter, which describes the sharpness of the band-edge states.

Luminescence Yield. The samples were excited by a 532 nm laser with different intensity from ~600 mW/cm^2 (6 suns) to ~4 × 10^6 mW/cm^2 (4 × 10^4 suns) to investigate the response of the as-grown InP films under various photon illumination. The external luminescence efficiency was calculated as

$$\eta_{ext} = (\phi_{InP}/\eta_{sys})/(\phi_{inc}T) \quad (3)$$

where ϕ_{inc} and ϕ_{InP} are the incident photon flux and the measured InP photon flux, respectively, T is the transmission coefficient at the air/InP boundary as measured *via* absorption measurements, and η_{sys} is the collection efficiency of the system for a Lambertian reference, which was a thick (>3 mm) Spectralon layer here.

Thereafter, the quasi-Fermi level splitting (ΔE_F) is calculated according to eq 1[9,48] where R_{abs} is the absorbed photon flux per unit area in the InP film, $a(E,\theta)$ is the absorbance of InP, and $b(E)$ is the blackbody spectrum at temperature T. The absorbance of InP was taken as $a(E,\theta) = a(E) \times T(\theta)$, where $a(E) = 1 - \exp(-2\alpha(E)L)$, with the absorption coefficient $\alpha(E) = 10^4$ cm^{-1} for $E > 1.344$ eV, $\alpha(E) = 10^4 \times \exp\left(\frac{E - E_g}{E_0}\right)$ cm^{-1} for $E < 1.344$ eV, L is the InP thickness, $E_g = 1.344$ eV is the band gap energy, E_0 is the Urbach parameter, and the angular-dependent $T(\theta)$ is the transmission coefficient as determined by the Fresnel equations. The blackbody spectrum was $b(E) = \frac{2n^2}{h^3c^2}E^2\left(\frac{1}{\exp\left(\frac{E}{kT}\right) - 1}\right)$. Here, n is the refractive index of air, h is Planck's constant, c is the light speed, k is the Boltzmann constant, and $T = 300$ K is the temperature.

ASSOCIATED CONTENT

Supporting Information

The Supporting Information is available free of charge on the ACS Publications website at DOI: 10.1021/acsnano.7b02124.

SEM images of indium evaporated on i-cone substrates with various evaporation conditions are shown in Figure S1; fabrication processes for i-cones with different depths are listed in Table S1 (PDF)

AUTHOR INFORMATION

Corresponding Author

*E-mail: rkapadia@usc.edu.

ORCID

Qingfeng Lin: 0000-0001-9367-1206
Zhiyong Fan: 0000-0002-5397-0129
Rehan Kapadia: 0000-0002-7611-0551

Notes

The authors declare no competing financial interest.

ACKNOWLEDGMENTS

The work was partially supported by a startup grant from USC Viterbi School of Engineering. R.K. acknowledges funding from the National Science Foundation (Award #1610604). The authors gratefully acknowledge the use of facilities at Dr. Brent Melot's Lab, Dr. Stephen Cronin's Lab, and Center for Electron

DOI: 10.1021/acsnano.7b02124
ACS Nano 2017, 11, 5113−5119

Microscopy and Microanalysis at University of Southern California for the results reported in this paper. Z.F. acknowledges the support by the General Research Fund (project 612113) from the Hong Kong Research Grant Council, the Hong Kong Innovation and Technology Fund (project ITS/362/14FP) from the Innovation and Technology Commission and National Natural Science Foundation of China (project 51672231). D.S. thanks the support by the USC Annenberg Graduate Fellowship.

REFERENCES

(1) Savin, H.; Repo, P.; von Gastrow, G.; Ortega, P.; Calle, E.; Garin, M.; Alcubilla, R. Black Silicon Solar Cells with Interdigitated Back-Contacts Achieve 22.1% Efficiency. *Nat. Nanotechnol.* **2015**, *10*, 624–628.

(2) Leung, S. F.; Yu, M.; Lin, Q. F.; Kwon, K.; Ching, K. L.; Gu, L. L.; Yu, K.; Fan, Z. Y. Efficient Photon Capturing with Ordered Three-Dimensional Nanowell Arrays. *Nano Lett.* **2012**, *12*, 3682–3689.

(3) Fan, Z. Y.; Kapadia, R.; Leu, P. W.; Zhang, X. B.; Chueh, Y. L.; Takei, K.; Yu, K.; Jamshidi, A.; Rathore, A. A.; Ruebusch, D. J.; Wu, M.; Javey, A. Ordered Arrays of Dual-Diameter Nanopillars for Maximized Optical Absorption. *Nano Lett.* **2010**, *10*, 3823–3827.

(4) Yu, R.; Lin, Q. F.; Leung, S. F.; Fan, Z. Y. Nanomaterials and Nanostructures for Efficient Light Absorption and Photovoltaics. *Nano Energy* **2012**, *1*, 57–72.

(5) Lee, M. H.; Takei, K.; Zhang, J. J.; Kapadia, R.; Zheng, M.; Chen, Y. Z.; Nah, J.; Matthews, T. S.; Chueh, Y. L.; Ager, J. W.; Javey, A. p-Type InP Nanopillar Photocathodes for Efficient Solar-Driven Hydrogen Production. *Angew. Chem., Int. Ed.* **2012**, *51*, 10760–10764.

(6) Qiu, Y. C.; Leung, S. F.; Zhang, Q. P.; Hua, B.; Lin, Q. F.; Wei, Z. H.; Tsui, K. H.; Zhang, Y. G.; Yang, S. H.; Fan, Z. Y. Efficient Photoelectrochemical Water Splitting with Ultrathin films of Hematite on Three-Dimensional Nanophotonic Structures. *Nano Lett.* **2014**, *14*, 2123–2129.

(7) Cui, Y.; van Dam, D.; Mann, S. A.; van Hoof, N. J. J.; van Veldhoven, P. J.; Garnett, E. C.; Bakkers, E. P. A. M.; Haverkort, J. E. M. Boosting Solar Cell Photovoltage *via* Nanophotonic Engineering. *Nano Lett.* **2016**, *16*, 6467–6471.

(8) Green, M. A. Radiative Efficiency of State-of-the-Art Photovoltaic Cells. *Prog. Photovoltaics* **2012**, *20*, 472–476.

(9) Miller, O. D.; Yablonovitch, E.; Kurtz, S. R. Strong Internal and External Luminescence as Solar Cells Approach the Shockley-Queisser Limit. *IEEE J. Photovolt.* **2012**, *2*, 303–311.

(10) Schnitzer, I.; Yablonovitch, E.; Caneau, C.; Gmitter, T. J. Ultrahigh Spontaneous Emission Quantum Efficiency, 99.7-Percent Internally and 72-Percent Externally, from AlGaAs/GaAs/AlGaAs Double Heterostructures. *Appl. Phys. Lett.* **1993**, *62*, 131–133.

(11) Sheng, X.; Yun, M. H.; Zhang, C.; Al-Okaily, A. M.; Masouraki, M.; Shen, L.; Wang, S. D.; Wilson, W. L.; Kim, J. Y.; Ferreira, P.; Li, X. L.; Yablonovitch, E.; Rogers, J. A. Device Architectures for Enhanced Photon Recycling in Thin-Film Multijunction Solar Cells. *Adv. Energy Mater.* **2015**, *5*, 1400919.

(12) Huang, H. T.; Lu, L. F.; Wang, J.; Yang, J.; Leung, S. F.; Wang, Y. Q.; Chen, D.; Chen, X. Y.; Shen, G. Z.; Li, D. D.; Fan, Z. Y. Performance Enhancement of Thin-Film Amorphous Silicon Solar Cells with Low Cost Nanodent Plasmonic Substrates. *Energy Environ. Sci.* **2013**, *6*, 2965–2971.

(13) Hsu, C. M.; Battaglia, C.; Pahud, C.; Ruan, Z. C.; Haug, F. J.; Fan, S. H.; Ballif, C.; Cui, Y. High-Efficiency Amorphous Silicon Solar Cell on a Periodic Nanocone Back Reflector. *Adv. Energy Mater.* **2012**, *2*, 628–633.

(14) Leung, S. F.; Gu, L. L.; Zhang, Q. P.; Tsui, K. H.; Shieh, J. M.; Shen, C. H.; Hsiao, T. H.; Hsu, C. H.; Lu, L. F.; Li, D. D.; Lin, Q. F.; Fan, Z. Y. Roll-to-Roll Fabrication of Large Scale and Regular Arrays of Three-Dimensional Nanospikes for High Efficiency and Flexible Photovoltaics. *Sci. Rep.* **2014**, *4*, 4243.

(15) Zhu, J.; Hsu, C. M.; Yu, Z. F.; Fan, S. H.; Cui, Y. Nanodome Solar Cells with Efficient Light Management and Self-Cleaning. *Nano Lett.* **2010**, *10*, 1979–1984.

(16) Lin, Q. F.; Hua, B.; Leung, S. F.; Duan, X. C.; Fan, Z. Y. Efficient Light Absorption with Integrated Nanopillar/Nanowell Arrays for Three-Dimensional Thin-Film Photovoltaic Applications. *ACS Nano* **2013**, *7*, 2725–2732.

(17) Lin, Q. F.; Leung, S. F.; Lu, L. F.; Chen, X. Y.; Chen, Z.; Tang, H. N.; Su, W. J.; Li, D. D.; Fan, Z. Y. Inverted Nanocone-Based Thin Film Photovoltaics with Omnidirectionally Enhanced Performance. *ACS Nano* **2014**, *8*, 6484–6490.

(18) Lin, Q. F.; Lu, L. F.; Tavakoli, M. M.; Zhang, C.; Lui, G. C.; Chen, Z.; Chen, X. Y.; Tang, L.; Zhang, D. Q.; Lin, Y. J.; Chang, P. C.; Li, D. D.; Fan, Z. Y. High Performance Thin Film Solar Cells on Plastic Substrates with Nanostructure-Enhanced Flexibility. *Nano Energy* **2016**, *22*, 539–547.

(19) Battaglia, C.; Hsu, C. M.; Soderstrom, K.; Escarre, J.; Haug, F. J.; Charriere, M.; Boccard, M.; Despeisse, M.; Alexander, D. T. L.; Cantoni, M.; Cui, Y.; Ballif, C. Light Trapping in Solar Cells: Can Periodic Beat Random? *ACS Nano* **2012**, *6*, 2790–2797.

(20) Zheng, M.; Wang, H. P.; Sutter-Fella, C. M.; Battaglia, C.; Aloni, S.; Wang, X. F.; Moore, J.; Beeman, J. W.; Hettick, M.; Amani, M.; Hsu, W. T.; Ager, J. W.; Bermel, P.; Lundstrom, M.; He, J. H.; Javey, A. Thin-Film Solar Cells with InP Absorber Layers Directly Grown on Nonepitaxial Metal Substrates. *Adv. Energy Mater.* **2015**, *5*, 1501337.

(21) Tavakoli, M. M.; Lin, Q. F.; Leung, S. F.; Lui, G. C.; Lu, H.; Li, L.; Xiang, B.; Fan, Z. Y. Efficient, Flexible and Mechanically Robust Perovskite Solar Cells on Inverted Nanocone Plastic Substrates. *Nanoscale* **2016**, *8*, 4276–4283.

(22) Tsui, K. H.; Lin, Q. F.; Chou, H. T.; Zhang, Q. P.; Fu, H. Y.; Qi, P. F.; Fan, Z. Y. Low-Cost, Flexible, and Self-Cleaning 3D Nanocone AntiRefl ection Films for High-Efficiency Photovoltaics. *Adv. Mater.* **2014**, *26*, 2805–2811.

(23) Lin, Q. F.; Huang, H. T.; Jing, Y.; Fu, H. Y.; Chang, P. C.; Li, D. D.; Yao, Y.; Fan, Z. Y. Flexible Photovoltaic Technologies. *J. Mater. Chem. C* **2014**, *2*, 1233–1247.

(24) Zheng, M.; Horowitz, K.; Woodhouse, M.; Battaglia, C.; Kapadia, R.; Javey, A. III-Vs at Scale: a PV Manufacturing Cost Analysis of the Thin Film Vapor-Liquid-Solid Growth Mode. *Prog. Photovoltaics* **2016**, *24*, 871–878.

(25) Chen, K.; Kapadia, R.; Harker, A.; Desai, S.; Seuk Kang, J.; Chuang, S.; Tosun, M.; Sutter-Fella, C. M.; Tsang, M.; Zeng, Y. P.; Kiriya, D.; Hazra, J.; Madhvapathy, S. R.; Hettick, M.; Chen, Y. Z.; Mastandrea, J.; Amani, M.; Cabrini, S.; Chueh, Y. L.; Ager, J. W.; et al. Direct Growth of Single-Crystalline III-V Semiconductors on Amorphous Substrates. *Nat. Commun.* **2016**, *7*, 10502.

(26) Ohring, M. *The Materials Science Of Thin Films*; Academic Press: Boston, MA, 1992.

(27) Wang, Z. L. Zinc Oxide Nanostructures: Growth, Properties and Applications. *J. Phys.: Condens. Matter* **2004**, *16*, R829–R858.

(28) Pan, Z. W.; Dai, Z. R.; Wang, Z. L. Nanobelts of Semiconducting Oxides. *Science* **2001**, *291*, 1947–1949.

(29) Wang, Z. L.; Song, J. H. Piezoelectric Nanogenerators Based on Zinc Oxide Nanowire Arrays. *Science* **2006**, *312*, 242–246.

(30) Chen, M. X.; Pan, C. F.; Zhang, T. P.; Li, X. Y.; Liang, R. R.; Wang, Z. L. Tuning Light Emission of a Pressure-Sensitive Silicon/ZnO Nanowires Heterostructure Matrix through Piezo-phototronic Effects. *ACS Nano* **2016**, *10*, 6074–6079.

(31) Rosenwaks, Y.; Shapira, Y.; Huppert, D. Evidence for Low Intrinsic Surface-Recombination Velocity on p-Type InP. *Phys. Rev. B: Condens. Matter Mater. Phys.* **1991**, *44*, 13097–13100.

(32) Zheng, M.; Yu, Z. B.; Joon Seok, T.; Chen, Y. Z.; Kapadia, R.; Takei, K.; Aloni, S.; Ager, J. W.; Wu, M.; Chueh, Y. L.; Javey, A. High Optical Quality Polycrystalline Indium Phosphide Grown on Metal Substrates by Metalorganic Chemical Vapor Deposition. *J. Appl. Phys.* **2012**, *111*, 123112.

(33) Joyce, H. J.; Docherty, C. J.; Gao, Q.; Tan, H. H.; Jagadish, C.; Lloyd-Hughes, J.; Herz, L. M.; Johnston, M. B. Electronic Properties of

DOI: 10.1021/acsnano.7b02124
ACS Nano 2017, 11, 5113–5119

GaAs, InAs and InP Nanowires Studied by Terahertz Spectroscopy. *Nanotechnology* **2013**, *24*, 214006.
(34) Duan, X. F.; Huang, Y.; Cui, Y.; Wang, J. F.; Lieber, C. M. Indium Phosphide Nanowires as Building Blocks for Nanoscale Electronic and Optoelectronic Devices. *Nature* **2001**, *409*, 66−69.
(35) Wallentin, J.; Anttu, N.; Asoli, D.; Huffman, M.; Aberg, I.; Magnusson, M. H.; Siefer, G.; Fuss-Kailuweit, P.; Dimroth, F.; Witzigmann, B.; Xu, H. Q.; Samuelson, L.; Deppert, K.; Borgstrom, M. T. InP Nanowire Array Solar Cells Achieving 13.8% Efficiency by Exceeding the Ray Optics Limit. *Science* **2013**, *339*, 1057−1060.
(36) Lee, W.; Schwirn, K.; Steinhart, M.; Pippel, E.; Scholz, R.; Gosele, U. Structural Engineering of Nanoporous Anodic Aluminium Oxide by Pulse Anodization of Aluminium. *Nat. Nanotechnol.* **2008**, *3*, 234−239.
(37) Lee, W.; Ji, R.; Gosele, U.; Nielsch, K. Fast Fabrication of Long-Range Ordered Porous Alumina Membranes by Hard Anodization. *Nat. Mater.* **2006**, *5*, 741−747.
(38) Lee, M. H.; Lim, N.; Ruebusch, D. J.; Jamshidi, A.; Kapadia, R.; Lee, R.; Seok, T. J.; Takei, K.; Cho, K. Y.; Fan, Z. Y.; Jang, H.; Wu, M.; Cho, G.; Javey, A. Roll-to-Roll Anodization and Etching of Aluminum Foils for High-Throughput Surface Nanotexturing. *Nano Lett.* **2011**, *11*, 3425−3430.
(39) Yu, R.; Ching, K. L.; Lin, Q. F.; Leung, S. F.; Arcrossito, D.; Fan, Z. Y. Strong Light Absorption of Self-Organized 3-D Nanospike Arrays for Photovoltaic Applications. *ACS Nano* **2011**, *5*, 9291−9298.
(40) Lin, Q. F.; Leung, S. F.; Tsui, K. H.; Hua, B.; Fan, Z. Y. Programmable Nanoengineering Templates for Fabrication of Three-Dimensional Nanophotonic Structures. *Nanoscale Res. Lett.* **2013**, *8*, 268.
(41) Lin, Y. J.; Lin, Q. F.; Liu, X.; Gao, Y.; He, J.; Wang, W. L.; Fan, Z. Y. A Highly Controllable Electrochemical Anodization Process to Fabricate Porous Anodic Aluminum Oxide Membranes. *Nanoscale Res. Lett.* **2015**, *10*, 495.
(42) Kapadia, R.; Yu, Z. B.; Wang, H. H. H.; Zheng, M.; Battaglia, C.; Hettick, M.; Kiriya, D.; Takei, K.; Lobaccaro, P.; Beeman, J. W.; Ager, J. W.; Maboudian, R.; Chrzan, D. C.; Javey, A. A Direct Thin-Film Path towards Low-Cost Large-Area III-V Photovoltaics. *Sci. Rep.* **2013**, *3*, 2275.
(43) Kapadia, R.; Yu, Z. B.; Hettick, M.; Xu, J. S.; Zheng, M. S.; Chen, C. Y.; Balan, A. D.; Chrzan, D. C.; Javey, A. Deterministic Nucleation of InP on Metal Foils with the Thin-Film Vapor-Liquid-Solid Growth Mode. *Chem. Mater.* **2014**, *26*, 1340−1344.
(44) Hua, B.; Lin, Q. F.; Zhang, Q. P.; Fan, Z. Y. Efficient Photon Management with Nanostructures for Photovoltaics. *Nanoscale* **2013**, *5*, 6627−6640.
(45) Massidda, S.; Continenza, A.; Freeman, A. J.; Depascale, T. M.; Meloni, F.; Serra, M. Structural and Electronic Properties of Narrow-Band-Gap Semiconductors: InP, InAs, and InSb. *Phys. Rev. B: Condens. Matter Mater. Phys.* **1990**, *41*, 12079−12085.
(46) Iribarren, A.; Castro-Rodriguez, R.; Sosa, V.; Pena, J. L. Band-Tail Parameter Modeling in Semiconductor Materials. *Phys. Rev. B: Condens. Matter Mater. Phys.* **1998**, *58*, 1907−1911.
(47) Iribarren, A.; Castro-Rodriguez, R.; Sosa, V.; Pena, J. L. Modeling of the Disorder Contribution to the Band-Tail Parameter in Semiconductor Materials. *Phys. Rev. B: Condens. Matter Mater. Phys.* **1999**, *60*, 4758−4762.
(48) Trupke, T.; Bardos, R. A.; Abbott, M. D.; Cotter, J. E. Suns-Photoluminescence: Contactless Determination of Current-Voltage Characteristics of Silicon Wafers. *Appl. Phys. Lett.* **2005**, *87*, 093503.
(49) Shockley, W.; Queisser, H. J. Detailed Balance Limit of Efficiency of p-n Junction Solar Cells. *J. Appl. Phys.* **1961**, *32*, 510−519.
(50) Wallentin, J.; Mergenthaler, K.; Ek, M.; Wallenberg, L. R.; Samuelson, L.; Deppert, K.; Pistol, M. E.; Borgstrom, M. T. Probing the Wurtzite Conduction Band Structure Using State Filling in Highly Doped InP Nanowires. *Nano Lett.* **2011**, *11*, 2286−2290.

DOI: 10.1021/acsnano.7b02124
ACS Nano 2017, 11, 5113−5119